Contents lists available at ScienceDirect

Environmental Pollution

journal homepage: www.elsevier.com/locate/envpol

Release of colloidal biochar during transient chemical conditions: The humic acid effect☆

Yang Wang [a], Scott A. Bradford [b], Jianying Shang [a, *]

[a] College of Land Science and Technology, China Agricultural University, Beijing, 100193, PR China
[b] US Salinity Laboratory, USDA, ARS, Riverside, CA, 92507, United States

ARTICLE INFO

Article history:
Received 7 October 2019
Received in revised form
16 January 2020
Accepted 23 January 2020
Available online 29 January 2020

Keywords:
Colloidal biochar
Release
Transient ionic strength
pH
Humic acid

ABSTRACT

Our understanding of colloidal biochar (CB) transport and release is largely unknown in environments with transient chemical conditions, e.g., ionic strength (IS), pH, and especially humic acid (HA). In this study, column experiments were conducted to investigate CB transport and retention in the presence and absence of HA, and CB release under transient IS and pH conditions in saturated sand. Step reductions in solution IS from 25 to 0.01 mM produced significant release peaks of CB due to a reduction in the depth of the primary minima on rough surfaces with small energy barriers. In contrast, step increases of solution pH from 4 to 10 only slightly increased CB release presumably due to the strong buffering capacity of CB. The CB retention was diminished by HA during the deposition phase. However, the release of CB with transients in IS and pH was not influenced much when deposition occurred in the presence of HA. These observations indicate that HA increased the energy barrier during deposition but did not have a large influence on the depth of the interacting minimum during transient release. Potential explanations for these effects of HA on CB retention and transient release include enhanced repulsive electrostatic interactions and/or altering of surface roughness properties. Our findings indicated that the release of retained CB is sensitive to transient IS conditions, but less dependent on pH increases and CB deposition in the presence of HA. This information is needed to quantify potential benefits and/or adverse risks of mobile CB in natural environments.

1. Introduction

Biochar, an artificially synthetic black carbon, can be used as a soil amendment to improve soil fertility, sequester carbon, and/or remediate contaminated soil and water (Lehmann and Joseph, 2015; Manyà, 2012; Qi et al., 2017). Biochar field application will inevitably release a small fraction of fine biochar particles (including nano- or micro-particles) into natural terrestrial and marine ecosystems (Joseph et al., 2013; Liu et al., 2019; Sigmund et al., 2018; Wang et al., 2013a). While some fine biochar particles may enter into surface water through runoff, drainage, and irrigation (Guggenberger et al., 2008; Zhang et al., 2010), other fine biochar particles may infiltrate into the soil and migrate downward through the vadose zone toward groundwater (Major et al., 2010). A portion of fine biochar particles in soils can be retained in the unsaturated and saturated subsurface environment, which may be released into soil solution as the solution chemical conditions change. Information related to the transport, retention, and release of fine biochar particles in the subsurface is important to evaluate the fate and potential long-term environmental risks (e.g., facilitated transport of contaminants) from biochar field application.

Release of colloids is dependent on the relative strengths of the adhesive interaction energy and random fluctuation in the kinetic energy of diffusing colloids, as well as the balance of the applied hydrodynamic and the resisting adhesive torques (Bradford et al., 2012; Bradford et al., 2015; Torkzaban et al., 2015). Under steady-state flow and stable physio-chemical conditions, small amounts of colloids can be slowly released by diffusion from the solid phase to the soil solution (Ryan and Elimelech, 1996; Ryan and Gschwend, 1994; Shen et al., 2007). Conversely, considerable amounts of colloids may be released during transient (i.e., temporal) changes of solution chemistry that diminish the adhesive interaction and/or the energy barrier to detachment (Bradford et al., 2015; Grolimund et al., 2001; Roy and Dzombak, 1996; Ryan and Elimelech, 1996; Torkzaban and Bradford, 2016). Tosco et al. (2009) and Chen et al.

☆ This paper has been recommended for acceptance by Yong Sik Ok.
* Corresponding author.
E-mail address: jyshang@cau.edu.cn (J. Shang).

https://doi.org/10.1016/j.envpol.2020.114068
0269-7491/

(2017) reported that chemical perturbations that induced detachment were well correlated with the disappearance of the secondary minimum (a shallow attractive well at a separation distance beyond the energy barrier in the interaction energy profile) under unfavorable attachment conditions. In addition, the surface roughness of the collector and the colloid plays a critical role in colloid retention and release (Bradford et al., 2017; Rasmuson et al., 2019; Shen et al., 2018; Torkzaban and Bradford, 2016), especially under low IS and high hydrodynamic torque conditions, by reducing the magnitudes of the secondary and primary minima (a deep attractive well at a small separation distance in the interaction energy profile) and the energy barrier height (Bradford and Torkzaban, 2015). Only limited research has studied the influence of transients in solution chemistry on biochar colloids release with a reduction in IS (Chen et al., 2017), but none for pH increases.

Natural dissolved organic matter such as humic acid (HA) is commonly found in the subsurface (Cheng et al., 2016; Fisher-Power and Cheng, 2018; Jansen et al., 2014; Yan et al., 2019). It normally shows less than 0.45 or 0.22 μm size fractions and contains a negative surface charge (Wang et al., 2016; Yang et al., 2017a; Yang et al., 2019a). Previous studies have demonstrated that HA can strongly facilitate the transport of colloidal particles, especially in relatively high ionic strength (IS) solutions (Roy and Dzombak, 1997; Ryan and Elimelech, 1996; Sen and Khilar, 2006; Yan et al., 2019; Yang et al., 2017b). This has been attributed to enhanced electrostatic repulsion (Li et al., 2008; Wang et al., 2008; Yang et al., 2017b) or steric repulsion (Fritz et al., 2002; Louie et al., 2012; Morales et al., 2011; Wang et al., 2013b) from adsorbed HA. Adsorbed HA can also facilitate colloid and nanoparticle release by altering the nanoscale surface roughness and chemical heterogeneity of both colloids and collector (Bradford et al., 2017; Kretzschmar and Sticher, 1997; Yang et al., 2019a). However, little research has investigated the influence of adsorbed HA on the release behavior of colloids, especially biochar colloids, under transient solution chemical conditions.

Overall objectives of this study were to investigate: (1) the release behavior of retained biochar colloids under transient solution IS and pH conditions; and (2) the effect of HA on the release of retained biochar colloids under these transient solution chemical conditions. Interaction energy calculations were conducted to study changes in the adhesive interaction and release mechanisms of colloidal biochar (CB) under various solution chemistry conditions, including the influence of HA and nanoscale roughness. A colloid release model that considered equilibrium and kinetic sites was used to simulate the observed CB release behavior and to quantitatively determine release rates. Understanding and predicting the subsurface transport and transient release of CB in the presence of HA can be used to optimize biochar application strategies and provides fundamental support for the rational long-term use of biochar in the field.

2. Materials and methods

2.1. Biochar preparation and characterization

Wheat straw (Zhengzhou, Henan Province, China) feedstock was heated to 600 °C at a constant rate of 20 °C min^{-1} and then kept at 600 °C for 1 h (Yang et al., 2017b). The obtained biochar sample was grounded into biochar powder (0.2–0.7 μm) using a ball mill (MM 400, Retsch, Germany). The pH and electrical conductivity (EC) of CB were determined in 1:5 suspensions of biochar in ultrapure water (Murray et al., 2015; Zhou et al., 2016). The ash content of the biochar was measured after heating in a muffle furnace at 750 °C for 6 h (ASTM, 2007). The C, N, O, and H concentrations in biochar were measured using an elemental analyzer (Flash 2000, Thermo Scientific, USA). The concentrations of minor elements were determined using an Inductively Coupled Plasma Optical Emission Spectrometer (ICP-OES, Avio 200, PerkinElmer, USA.) after digesting the biochar sample in a mixture of nitric acid (HNO_3) and perchloric acid ($HClO_4$) (Kalra, 1997). The functional groups of biochar were well characterized by Fourier transformation infrared (FTIR, Spectrum Spotlight 200, PerkinElmer, USA) and X-ray photoelectron spectroscopy (XPS, Thermo Fisher Scientific K-Alpha, Thermo Fisher, USA).

The stock suspension of CB was prepared by adding biochar powder into ultrapure water and then sonicating for 30 min before use (Wang et al., 2013a). The morphology of CB was determined using transmission electron microscopy (TEM, JEOL JEM-1230, JEOL. Ltd, Japan). The zeta potential and hydrodynamic particle size distribution of the CB in a selected solution chemistry were measured using a Zetasizer (Nano ZS90, Malvern, UK). The surface roughness of CB was measured by atomic force microscopy (AFM, Dimension Edge, Bruker, Germany), and the static contact angles of biochar were determined by the sessile drop method using a goniometer (JC2000D2, POWEREACH, China) at 25 °C (Yang et al., 2017b).

2.2. Porous media and electrolyte solutions

Quartz sand (Sinopharm, Beijing, China) with size ranging from 425 to 600 μm was used as the porous medium in column experiments. The quartz sand was immersed in 36–38% HCl solution to remove organic matter and Fe/Al oxides on the surface. The sand was washed repeatedly by ultrapure water until the conductivity of the wash water was close to that of the ultrapure water. The sand was dried in an oven at 105 °C for 24 h and then baked in a muffle furnace at 600 °C for 4 h (Chen et al., 2015). The surface morphology and roughness of the quartz sand were determined using a scanning electron microscope (SEM, FEI FIB 200, FEI Technologies Inc., Oregon, USA).

Electrolyte solutions were prepared using NaCl at IS of 0.01, 0.1, 1, 5, 10 and 25 mM. The pH of the electrolyte solutions was adjusted using either 0.1 M HCl or 0.1 M NaOH to obtain a pH of 4 or 7, and the NaCl solution at pH 10 was adjusted using a buffer solution of $NaHCO_3$ and NaOH (Bradford et al., 2015). The stock solution of HA (pH 6.9, Sigma Aldrich, USA) was prepared in ultrapure water and sonicated for 10 min to obtain better dispersion, and then passed through a 0.45 μm nylon membrane filter (Jinlong, Tianjin, China) before use.

2.3. Column experiments

Stainless steel columns (length of 12.6 cm and inner diameter of 2.6 cm) were used in the transport experiments. Nylon mesh (80-mesh, Jie Rong, Hangzhou, China) was placed at both the ends of the column to support the quartz sand and disperse the water flow. The average bulk density and porosity of the packed column were ~1.45 g cm^{-3} and ~0.45, respectively. The column experiments were run in an up-flow mode using a peristaltic pump (DHL-A, Huxi, Shanghai, China), and the average pore water velocity was 0.41 cm min^{-1}. One pore volume (PV) corresponds to a residence time of 0.5 h in the column. The column was pre-equilibrated by injecting at least 5 PVs of the desired electrolyte solution. Following the pre-equilibration, 5 PVs of 250 mg L^{-1} CB in the absence/presence of 10 mg L^{-1} HA were injected into the column (Phase 1) and then 4 PVs of biochar-free background electrolyte solution (Phase 2). To investigate the release behavior of the retained CB under transient solution chemistry conditions, the columns were systematically flushed by changing the influent solution chemical conditions in 3–10 PVs steps.

Experiments were designed to examine the effect of IS reduction or pH increase on the release of retained CB. Solution chemistry sequences were selected so that the average surface interaction of biochar and quartz sand was increasingly unfavorable for attachment (Table 1). In IS reduction experiments the CB was deposited during Phase 1 in 25 mM NaCl at a neutral pH (7.6 or 7.2) in the absence (denoted as IS column) or presence of 10 mg L^{-1} HA (denoted as IS_HA column). Next, the influent solution IS was sequentially reduced from 25 mM (Phase 1 and 2) to 5 mM (Phase 3a), 1 mM (Phase 3b), 0.1 mM (Phase 3c), and then 0.01 mM (Phase 3d). Experiments with pH were conducted by depositing CB during Phase 1 in the absence (denoted as pH column) or presence of 10 mg L^{-1} HA (denoted as pH_HA column) when the solution pH = 4 and the IS = 10 mM NaCl. Next, the influent solution pH was sequentially increased from 4 (Phase 1 and 2) to 7 (Phase 3a), and then 10 (Phase 3b) while keeping the IS = 10 mM NaCl. The pH of the effluents was monitored continuously as the inflow pH was changed from 4 to 10 during the whole experiment. The effluent samples were collected every 5 min by a fraction collector (BSZ-100, Huxi, Shanghai, China). Detailed column information is presented in Table 1 and Table S1.

The spatial distribution of CB in each column was determined at the end of column experiments. The sand was carefully excavated in 1 cm increments and placed into 20 mL ultrapure water in 50-mL glass flasks. The glass flasks were shaken at 120 rpm for 4 h to liberate the retained CB from the sand surface. The concentration of CB was measured by UV-VIS spectrophotometer at the wavenumber of 790 nm. A calibration curve of CB was provided in Fig. S1. Replicate experiments were conducted and exhibited good reproducibility.

2.4. Interaction energies

The transport, retention, and release of CB under transient solution chemistry conditions are highly dependent on adhesive interactions of CB with the quartz sand. Extended Derjaguin-Landau-Verwey-Overbeek (XDLVO) calculations were therefore conducted to determine the total interaction energy between CB and quartz sand. These calculations included the sum of Lifshitz-van der Waals (LW), electric double layer repulsion (EDL) and Lewis acid-base (AB) interactions for a sphere-plate geometry (Gregory, 1981; van Oss et al., 1988; van Oss, 2003). The steric force was not considered in these calculations because it predicts a large energy barrier to CB interactions with the quartz sand that is not consistent with our experimental observations. The detailed information pertaining to the XDLVO interaction energy calculations are shown in the Support Information.

2.5. Steady-state colloid transport model

The transport of CB in a saturated quartz sand column was simulated using the HYDRUS 1D software package (Simůnek et al., 2008). HYDRUS 1D solves the one-dimensional convection-dispersion equation with terms for kinetic exchange to/from the aqueous and the solid phases as:

$$\frac{\partial \theta_w C}{\partial t} = \frac{\partial}{\partial_z}\left(\theta_w D \frac{\partial C}{\partial z}\right) - \frac{\partial q_w C}{\partial z} - \theta_w \psi k_{sw} C + \rho_b k_{rs} S \quad [1]$$

where θ_w [L^3 L^{-3}; where L denotes units of length] is the volumetric water content, C [N L^{-3}; where N denote the number] is the concentration of CB in the aqueous phase, D [L^2 T^{-1}; where T denotes units of time] is the hydrodynamic dispersion coefficient for CB, q_w [$L T^{-1}$] is the Darcy water velocity of our experiment, k_{sw} [T^{-1}] is the CB retention rate coefficient (Phase 1 & 2); k_{rs} [T^{-1}] is the CB steady-state release rate coefficient (Phase 1 & 2), ρ_b [M L^{-3}; where M denotes units of mass] is the bulk density of the sand column, S [N M^{-1}] is the CB concentration on the solid phase, ψ [-] is a dimensionless Langmuirian blocking function that is equal to 1-S/S_{max} (e.g., Adamczyk et al., 1994) where S_{max} [N M^{-1}] is the maximum CB concentration in the solid phase. The solid phase mass balance is also calculated using the last two terms on the right-hand side of Eq. [1].

2.6. Equilibrium and kinetic model

The HYDRUS 1D software package was also used to simulate CB release during Phase 3 (transient conditions). In this case, the convective dispersion equation (Eq. [1]) was used to describe CB transport with $k_{sw} = k_{rs} = 0$, and transient release from the solid phase was modeled using the approach of Bradford et al. (2015). Equations for equilibrium and kinetic transient release from the

Table 1
The zeta potentials of CB and sand, hydrodynamic size of CB in effluents, and XDLVO interaction energy parameters for CB-sand interactions. The standard deviations with the zeta potentials and hydrodynamic size were shown in the parenthesis.

Experiments	Phase	IS [a] mM	PV [b]	HA [c] mg L^{-1}	pH[d]	ζ^e_{CB} mV	ζ^f_S mV	Hydrodynamic size[g] nm	Φ^h_{max} kT	Φ^i_{min2} kT
IS column	1 & 2	25	0–9	0	7.6	−26.6 (3.6)	−41.5 (0.8)	504.5 (30)	11.5	−0.34
	3a	5	10–13	0	7.6	−49.8 (1.0)	−50.9 (1.3)	415.2 (9)	299.6	−0.04
	3b	1	14–17	0	7.6	−52.2 (1.0)	−52.7 (1.4)	388.8 (11)	516.8	−0.01
	3c	0.1	18–23	0	7.6	−39.8 (1.3)	−54.6 (1.1)	363.2 (7)	476.7	–
	3d	0.01	24–28	0	7.6	−43.5 (0.2)	−56.1 (0.5)	361.2 (10)	591.0	–
IS_HA column	1 & 2	25	0–9	10	7.2	−28.9 (3.7)	−44.7 (1.0)	475.2 (8)	15.4	−0.27
	3a	5	10–13	10	7.2	−50.5 (2.2)	−53.5 (1.5)	395.7 (8)	309.1	−0.04
	3b	1	14–17	10	7.2	−53.2 (1.0)	−55.9 (0.9)	378.8 (11)	547.8	−0.01
	3c	0.1	18–23	10	7.2	−42.4 (1.1)	−56.7 (1.4)	358.7 (9)	526.2	–
	3d	0.01	24–28	10	7.2	−45.7 (0.4)	−58.1 (0.9)	355.6 (8)	637.0	–
pH column	1 & 2	10	0–9	0	4.0	−35.2 (2.3)	−30.6 (1.5)	448.8 (15)	59.9	−0.11
	3a	10	10–16	0	7.0	−45.5 (1.8)	−45.1 (1.8)	428.5 (12)	146.2	−0.08
	3b	10	17–23	0	10.0	−45.6 (2.8)	−47.3 (1.9)	417.0 (16)	160.6	−0.09
pH_HA column	1 & 2	10	0–9	10	4.0	−36.0 (0.9)	−31.3 (2.0)	438.3 (12)	62.3	−0.10
	3a	10	10–16	10	7.0	−46.1 (1.3)	−46.4 (2.6)	420.5 (8)	152.2	−0.09
	3b	10	17–23	10	10.0	−46.7 (1.2)	−48.8 (1.7)	408.5 (11)	162.0	−0.08

[a,b,c,d]Ionic strength (IS), pore volume (PV), humic acid (HA), and the pH in injection solution.
[e,f]The ζ potentials of the colloidal biochar and sand, respectively.
[g]Average hydrodynamic size of colloidal biochar measured by DLS.
[h,i]The maximal energy barrier and secondary energy minimum calculated by the XDLVO theory, respectively.

solid phase are shown below.

$$\rho_b \frac{\partial S_{eq}}{\partial t} = \rho_b S_i F_{eq} \frac{\partial f_{nr}}{\partial t} H_0 \left(- \frac{\partial f_{nr}}{\partial t} \right) \quad [2]$$

$$\rho_b \frac{\partial S_{k1}}{\partial t} = - \rho_b k_{det1} (S_{k1} - F_{k1} f_{nr} S_i) H_0 (S_k - F_{k1} f_{nr} S_i) \quad [3]$$

where S_{eq} [N M^{-1}], S_{k1} [N M^{-1}], and S_i [N M^{-1}] are the equilibrium, kinetic and initial (start of Phase 3) concentrations of retained CB in the sand surface, respectively; F_{eq} and F_{k1} are the fraction of equilibrium sites and kinetic sites, respectively; f_{nr} is the fraction of the retained CB that is not released by the chemical alteration, and H_0 is a Heaviside function that equals 1 during a chemical perturbation and is otherwise 0. Note that f_{nr} is a function of solution chemistry. It was determined by linear interpolation of experimental mass balance values following step changes in solution chemistry.

3. Results and discussion

3.1. Characteristics of biochar colloids

The biochar pH is 9.7, the EC is 10.6 mS cm^{-1}, and the total ash content is 20.7%. The element composition of biochar included 59.4% C, 37.9% O, 1.8% H, and 0.9% N. The minor elements were K (63.7 mg g^{-1}), Na (38.3 mg g^{-1}), Ca (25.6 mg g^{-1}), Mg (10.0 mg g^{-1}), Fe (16.7 mg g^{-1}), Al (9.8 mg g^{-1}), Si (5.2 mg g^{-1}), and Zn (4.1 mg g^{-1}). The spectral analysis of FTIR and XPS (Fig. 1) showed that biochar contained considerable hydroxyl, carboxyl, phenol and aromatic functional groups. The biochar surface was hydrophobic; e.g., biochar contact angles with water, glycerol, and n-decane were 122.6° ± 3°, 99.7° ± 8.4°, and 0°, respectively (Yang et al., 2017b).

TEM images showed that the shape of the CB was irregular (Fig. 2a). The hydrodynamic particle size of the CB ranged from 170 to 700 nm with an average of 380 nm and a standard deviation of 54 nm (Fig. 2b). AFM images demonstrated that the surface of CB was very rough (Fig. 2c and d). The surface roughness of CB was in the range of 3.0–14.7 nm, and the arithmetical mean deviation (Ra) of surface roughness was about 14.2 nm.

3.2. Transport and retention of CB in the presence and absence of HA

Figs. 3 and 4 present observed and simulated CB breakthrough curves (BTCs) in the absence/presence of HA when the IS = 25 mM NaCl and the pH = 7.6 or 7.2 (Fig. 3) and the IS = 10 mM NaCl and the pH = 4 (Fig. 4). Table 2 provides a summary of fitted model parameters (k_{sw}, k_{rs}, and S_{max}/C_o) during Phase 1 and 2, and the correlation coefficient for the goodness of fit (R^2). The value of R^2 was always greater than 0.86, indicating that the reversible Langmuirian blocking model provided a reasonable description of these BTCs.

Fig. 3 indicates that the CB breaks through at 1 PV and does not exhibit retardation or size exclusion. Next, the effluent concentrations continuously increase with CB injection and do not exhibit a plateau phase. This behavior has been attributed to blocking behavior (filling of available retention sites) that is well captured by the blocking model. The effluent concentration rapidly decreases to background levels during Phase 2, indicating that little detachment occurred during steady-state flow and solution chemistry conditions.

Mass balance information for these experiments is provided in Table S2. Effluent mass balance equaled 4.9%, 13.1%, 37.2%, and 47.6% for the IS column, IS_HA column, pH column, and pH_HA experiments, respectively. This corresponds to a solid phase mass balance of 95.1%, 86.9%, 62.8%, and 52.4% for these same systems. Similarly, the values of k_{sw} and S_{max}/C_o followed this same order in Table 2. Clearly, considerable amounts of CB retention occurred in all experiments, but especially at higher IS and in the absence of HA. Greater amounts of CB retention are expected at higher IS because of compression of the double layer thickness that reduces the energy barrier to interaction in a primary minimum (Table 1). The secondary minimum was always much less than the average kinetic energy of diffusing colloids (around 1.5 kT) (Hahn and O'Meliae, 2004) and was therefore viewed to play an insignificant role in CB retention. The presence of HA diminished CB retention and increased the blocking effect at a given IS condition due to alteration of the electrostatic interaction. In particular, the zeta potential of the sand and the CB became more negative in the presence of adsorbed HA, and this increased the energy barrier to interaction in the primary minimum (Table 1). This has previously been attributed to the strong adsorption of HA on biochar surfaces (Chen et al., 2017; Yang et al., 2017a; Yang et al., 2017b).

It should be mentioned that the predicted energy barrier to CB interaction with the quartz sand was always >11.5 kT (Table 1). The Boltzmann and Maxwellian models predict that this energy barrier is sufficiently high to inhibit CB from diffusing over this barrier into a primary minimum (Bradford et al., 2017). However, the XDLVO calculations presented in Table 1 assumed smooth and chemically homogeneous CB and quartz sand. Fig. 2c and d shows that the CB

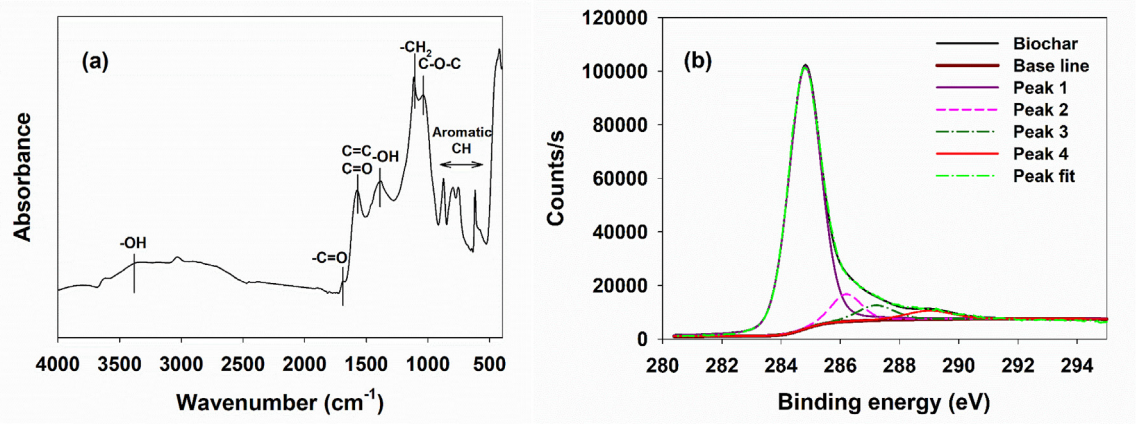

Fig. 1. The FTIR spectra and XPS (C1s region scan) of the biochar. The C1s spectra included C–C, C–H, or C=C (aromatic carbon, 82%) at peak 1 of ~284.6 eV, C–O (phenolic hydroxyl or ether group, 8.1%) at peak 2 of ~286.2 eV, C=O (ketone C, 5.4%) at peak 3 of ~287.2 eV, and O=C–O (carboxylic group, 3.9%) at peak 4 of ~289.0 eV.

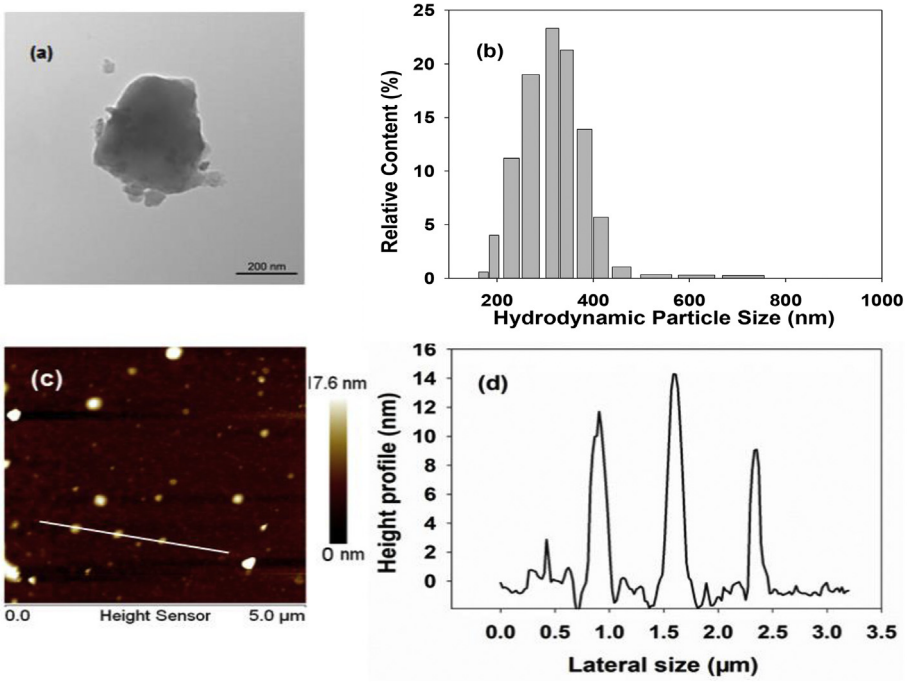

Fig. 2. (a) TEM image and (b) hydrodynamic particle size distribution, (c) AFM image of CB, and (d) the diameter and thickness analysis of CB on the line in the AFM image (c).

surface is rough with a roughness indicator Ra of 14.19 nm. Similarly, other researchers have found that the biochar surface was very rough through small-angle X-ray scattering, SEM and TEM analysis (Dong et al., 2017; Rechberger et al., 2017; Yang et al., 2019a). Furthermore, quartz sand surfaces are reported to be very rough (Li et al., 2017). Interaction energy calculations have shown that a small degree of surface roughness can significantly reduce or eliminate the height of the energy barrier (approximately two orders of magnitude) to the primary minimum (Bradford et al., 2017). Charge heterogeneity on the CB and/or quartz sand may also reduce or eliminate the energy barrier to the primary minimum (Jacob et al., 2015; Shen et al., 2007; Wen et al., 2014). Therefore, surface roughness and surface heterogeneity are expected to be important factors contributing to the large amount of CB retention on the sand surface (Bradford and Leij, 2018; Bradford and Torkzaban, 2013; Li et al., 2017; Shen et al., 2007; Torkzaban and Bradford, 2016). Note that consideration of steric effects from adsorbed HA predicts a huge energy barrier to the primary minimum and no CB retention (Chen et al., 2012; Hwang et al., 2018). This prediction is not consistent with our experimental observations of significant retention and was therefore not considered further.

3.3. Transport and release of CB with transients in solution chemistry

Fig. 3 presents effluent CB concentrations when the influent solution pH was neutral and the IS was sequentially reduced from 25 (Phase 1 and 2) to 5 (Phase 3a), 1 (Phase 3b), 0.1 (Phase 3c), and 0.01 (Phase 3d) mM NaCl in a stepwise manner. Fig. 4 presents similar information when the solution IS = 10 mM NaCl and the influent solution pH was sequentially increased in a stepwise manner from pH = 4 (Phase 1 and 2) to 7 (Phase 3a) and then to 10 (Phase 3b). Phase 1 was conducted in the absence and presence of HA in Figs. 3a and 4a, and Figs. 3b and 4b, respectively. Table S2 provides mass balance information for these release experiments. About 8.7%, 7.3%, 2.3%, and 3.5% of the injected CB mass was recovered during Phase 3 for IS column, IS_HA column, pH column, and pH_HA experiments, respectively.

Step reductions in IS and increases in pH both produced release pulses of CB (Figs. 3 and 4). However, the peak concentration of the release pulse was much greater for reductions in IS than an increase in pH. In fact, reductions in IS produced peak CB concentrations in the release pulses that were similar to or greater than the maximum value during Phase 1. A transient reduction in solution IS (e.g., infiltration and recharge) may therefore remobilize significant amounts of retained CB. Conversely, the presence of adsorbed HA during Phase 1 did not have a large influence on the mass of CB release during Phase 3 for either IS reductions or pH increases (<1.4% difference in injected mass).

Table 1 indicates that the secondary minimum was negligible for the CB. Previous studies have demonstrated that the secondary minimum can contribute to colloid deposition when it is larger than the average thermal energy (~1.5 kT) of Brownian particles (Hahn and O'Meliae, 2004; Bradford et al., 2017; Chen et al., 2018; Feke and Prabhu, 1985; Redman et al., 2004; Shen et al., 2007; Shen et al., 2018; Tufenkji and Elimelech, 2004; Yang et al., 2017b). In this study, the secondary minima were much less than 1.5 kT (Table 1), so it has negligible influence. Consequently, the retained CBs are expected to interact in a primary minimum during release experiments. Note that the energy barrier to CB detachment (difference in the energy barrier height and the depth of the primary minimum) on the smooth surface was always greater than 10 kT (Shen et al., 2018). Consequently, no CB detachment by diffusion is predicted for these conditions. Furthermore, the energy barrier to detachment is predicted to increase with a decrease in IS or an increase in pH on a smooth surface (Table 1). In contrast to experimental observations in Figs. 3 and 4, a decrease in IS or increase in pH should therefore decrease CB release from a smooth surface. Similarly, Shen et al. (2018) demonstrated that nanoscale charge heterogeneity cannot explain an increase in colloid and nanoparticle (NP) release with a decrease in IS because the primary minimum is very deep on a smooth surface. Interaction energy

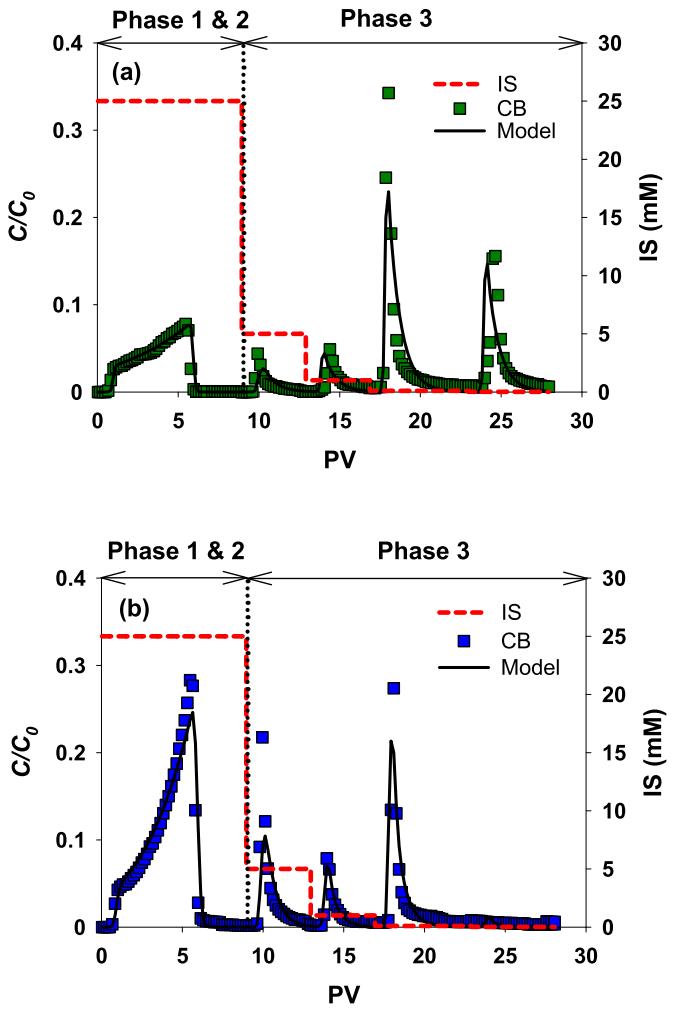

Fig. 3. The observed and fitted breakthrough and release curves of CB in the (a) absence and (b) presence of 10 mg L^{-1} HA at pH 7.6/7.2 under transient IS condition. CB was initially injected and flushed in 25 mM NaCl solution during Phase 1 and 2, and then the IS was continuously decreased from 25 to 5, 1, 0.1, 0.01 mM during Phase 3. The fitted parameters were shown in Tables 2 and 3.

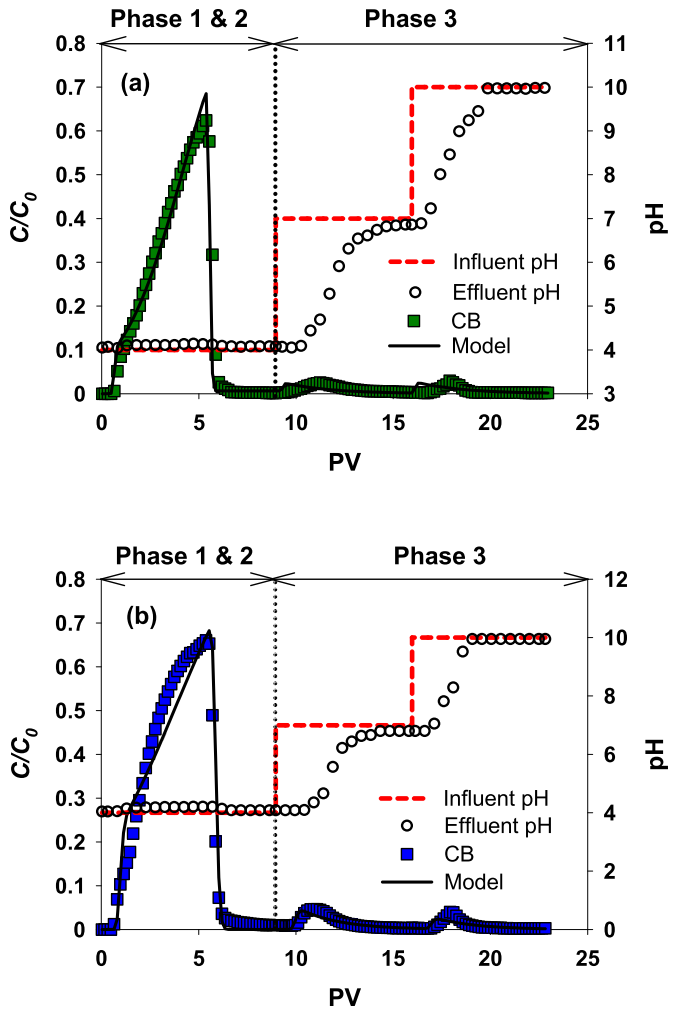

Fig. 4. The observed and fitted breakthrough and release curves of CB in the (a) absence and (b) presence of 10 mg L^{-1} HA in 10 mM NaCl solutions under transient pH condition. During Phase 1 & 2, the solution pH was set at 4, and during Phase 3 the solution pH was continuously changed to 7 (Phase 3a) and 10 (Phase 3b).

calculations have predicted colloid and NP release for certain rough conditions with a decrease in IS (Torkzaban and Bradford, 2016; Shen et al., 2018) or an increase in pH (Torkzaban and Bradford, 2016) due to a reduction in energy barrier to detachment to levels that allow for diffusive release (Figs. S3 and S4). Furthermore, the roughness conditions that produce colloid and NP release changes with the solution chemistry due to a reduction and/or elimination of the energy barrier and the creation of a shallow primary minimum (Bradford et al., 2017; Bradford and Torkzaban, 2013; Li et al., 2017; Shen et al., 2012; Wang et al., 2019). Extensive surface roughness exists on both colloid and collector surfaces (Fig. 2 and S2). Nanoscale roughness may therefore provide a viable explanation for the discrepancy between XDLVO predictions for smooth surfaces and experimental observations of release from rough surfaces with a reduction in IS or an increase in pH.

Figs. 3 and 4 indicate that CB release was more sensitive to a reduction in IS from 25 to 0.01 mM at neutral pH than to increases in pH from 4 to 10 at an IS = 10 mM. Several factors can contribute to this difference in release. For example, the initial conditions for CB release were very different in transient IS and pH experiments (Fig.S5 and S6). Greater amounts of CB retention and higher values of S_{max}/C_o occurred in Phase 1 of the IS than the pH column

Table 2
Fitted model parameters to the CB breakthrough curves during Phase 1 and 2. The standard errors associated with the parameter were given in the parenthesis.

Experiments	k_{sw}[a] min^{-1}	k_{rs}[b] min^{-1}	S_{max}/C_0[c] $cm^3\ g^{-1}$	R^2
IS column	0.1178 (0.0035)	0 (0.0001)	19.69 (0.57)	0.86
IS_HA column	0.1045 (0.0036)	0 (0.0001)	8.68 (0.08)	0.94
pH column	0.1128 (0.006)	0 (0.0001)	1.60 (0.04)	0.96
pH_HA column	0.0464 (0.0024)	0.0001 (0.0002)	4.14 (0.04)	0.96

[a] The retention rate coefficient.
[b] The steady-state release rate coefficient.
[c] The ratio of the maximum solid phase concentration (S_{max}) of retained colloidal biochar to the initial colloid concentration (C_0) in the aqueous phase.

experiments (Table 2 and S2). This implies that a wider range of roughness conditions contributed to CB retention and greater release in the IS column experiments. In addition, a reduction in IS and an increase in pH both create more negative zeta potentials on the sand and the CB (Table 1), whereas a reduction in IS can also contribute to enhanced release by diminishing the depth of the primary minimum when the double layer thickness is expanded (Bradford et al., 2012; Pazmino et al., 2014; Shen et al., 2018; Torkzaban et al., 2015). Furthermore, CB release in the pH column

and pH_HA experiments may have been inhibited by the strong buffering ability of biochars (Smider and Singh, 2014; Wang et al., 2017; Yang et al., 2015; Yang et al., 2019a) which caused the effluent pH to slowly change over time (especially within the gap between CB and sand), even after the influent pH was changed for more than 1 PV (Fig. 4).

3.4. Mathematical modeling of transient CB release

Figs. 3 and 4 also show the simulated release behavior of CB with IS reduction and pH increase, respectively. Fig. 5 provides the values of f_{nr} that were determined from mass balance information that was used in these simulations. Values of f_{nr} occur over a relatively narrow range from 1 to 0.88 for IS reductions and from 1 to 0.93 for pH increases. A reduction in IS had a larger influence (decrease) on f_{nr} at lower IS, whereas an increase in pH produced almost a linear decrease in f_{nr}. Similar observations have been reported in the literature for bacteria release (Bradford et al., 2015). In addition, values of f_{nr} were slightly higher in the absence than in the presence of HA at given IS and pH conditions. This implies that when the IS of the solution was reduced or the pH was increased, the retention of CB in the presence of HA during Phase 1 slightly increased the subsequent release. In this case, adsorbed HA caused a more negative surface charge (Table 1) and possibly steric repulsion to create a larger repulsive interaction between HA-adsorbed CB and grain surfaces (Yang et al., 2019a).

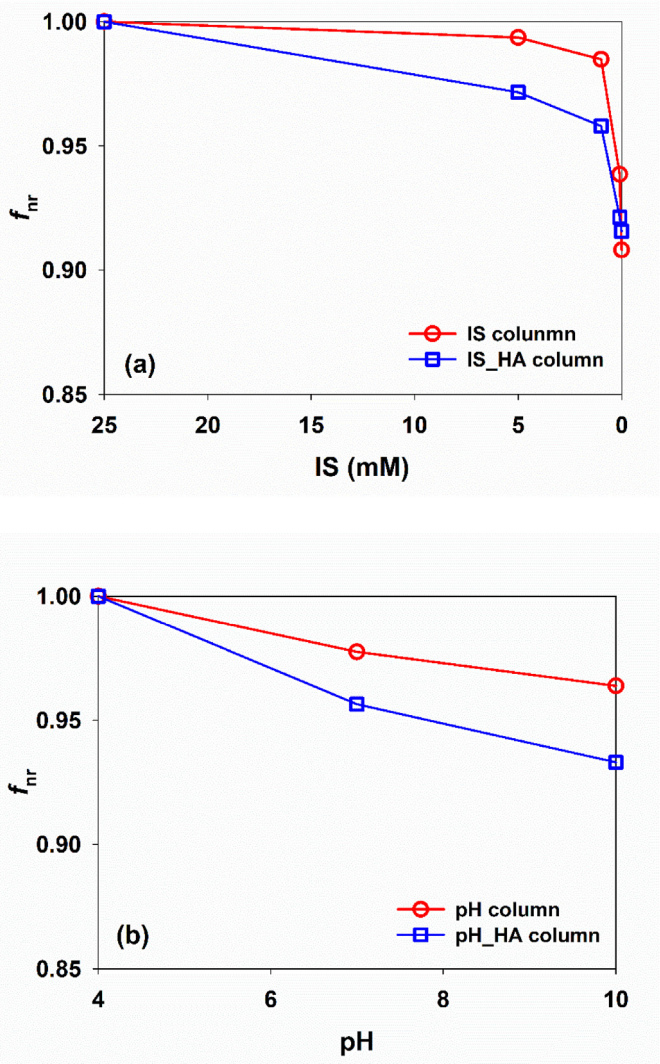

Fig. 5. The values of f_{nr} as a function of transient IS and pH conditions for CB in the absence and presence of 10 mg L^{-1} HA in the IS column and IS_HA column (Fig. 5a), pH column and pH_HA experiments (Fig. 5b). In Fig. 5a, the CB was initially deposited in 25 mM NaCl solution, and the IS conditions were successively altered in Phase 3. In Fig. 5b, the CB was initially deposited in the 10 mM NaCl solution at pH = 4, and the pH conditions were continuously changed in Phase 3.

Table 3 gives the fitted values of k_{det1} and F_k (F_{eq} = 1-F_k), as well as the R^2. The two-site release model always provided a reasonable description of the experimental data ($R^2 > 0.73$). Both equilibrium and kinetic release sites were needed to describe CB release with IS reduction. In this case, most of the release sites were kinetic ($F_k > 0.615$) and had relatively high values of k_{det1} equal to 0.045 min^{-1} (without HA) to 0.055 min^{-1} (with HA). Even faster release occurred from the remaining equilibrium site, and greater numbers of equilibrium sites occurred in the presence ($F_{eq} = 0.38$) than the absence ($F_{eq} = 0.1$) of HA. The presence of HA, therefore, increased the number of sites that undergo rapid release. This can be attributed to: (1) increased repulsive electrostatic and steric interactions from adsorbed HA (Yang et al., 2019b); and (2) the reduction and/or elimination of the energy barrier energy due to surface roughness of CB. Conversely, only a single kinetic site was needed to describe the pH release experiments ($F_k = 1$). In this case, the value of k_{det1} was much lower for pH increase than with IS reduction. The presence of HA during Phase 1 only slightly increased the kinetics of CB release with pH increase, presumably due to the strong buffering capacity of colloidal biochar.

Although the presence of HA diminished CB retention during Phase 1 (Table S2), it only had a relatively minor influence on the mass of CB release during Phase 2 and 3 (Table S2). However, adsorbed HA does appear to increase the rate of CB release (Table 3). This implies that adsorbed HA on the CB sometimes created a shallower depth of the primary minimum that was subject to a faster rate of diffusive release. Adsorbed HA will alter the surface roughness properties, and this can potentially lower the energy barrier and create shallower primary minimum interactions (Bradford et al., 2017) with higher release rates.

3.5. Spatial distributions of retained CB

Following the completion of Phases 1–3 (Figs. 3 and 4), the spatial distribution of retained CB was measured. These retention profiles are shown in Figs. S7 and S8. Note that the vast majority of retained CB could be recovered from the sand by resuspending in ultrapure water and shaking for 4 h (Table S2). Shaking the sand destroys the pore structure and continuously alters the lever arms that act on retained CB (Chen et al., 2017; Wang et al., 2013a; Wang et al., 2019). In this case, CB that are retained by surface and/or pore straining processes can be liberated by alteration of the torque balance (lever arms) at grain-grain contacts and at microscope

Table 3
Model parameters for the CB release curve during Phase 3. The standard errors were given in the parenthesis.

Experiments	Model[a]	k_{det1}[b] min^{-1}	F_{eq}[c]	F_k[d]	R^2
IS column	EK	0.045 (0.004)	0.10 (0.03)	0.901	0.73
IS_HA column	EK	0.055 (0.008)	0.38 (0.05)	0.615	0.89
pH column	EK	0.013 (0.006)	0.0	1	0.97
pH_HA column	EK	0.016 (0.006)	0.0	1	0.97

[a] The model used in our study was equilibrium and kinetic model (EK), in which site 1 was equilibrium and site 2 was kinetic.
[b] The release rate coefficient.
[c] The fraction of equilibrium sites.
[d] The fraction of kinetic sites that was equal to F_k = 1-F_{eq}.

roughness locations (Bradford et al., 2013; Tufenkji et al., 2004). A relatively small percentage of the CB were irreversibly retained on the sand and could not be recovered during this excavation process (<17.3%). These irreversibly retained CB are expected to be interacting in a strong primary minimum which can occur on smooth surfaces with charge heterogeneity and/or in crevice sites (Li et al., 2017).

4. Conclusions

Column experiments and mathematical modeling were conducted to examine the influence of IS reduction and pH increase on the release of colloidal biochar that was retained in the presence and absence of humic acid. A significant portion of the retained colloidal biochar was released when the solution IS was reduced, and deposition in the presence of humic acid accelerated this release process. In contrast, a change of solution pH from acidic to alkaline conditions only caused the slight release of retained colloidal biochar even in the presence of humic acid, presumably due to the strong buffering capacity of the colloidal biochar. Humic acid significantly diminished the retention of colloidal biochar but did not have a large influence on release during IS reduction or pH increase.

Interaction energy calculations were used to interpret the experimental observations. The secondary minimum for the colloidal biochar was insignificant and was therefore not considered to play an important role in retention or release. Conversely, colloid biochar retention in a primary minimum was possible on surfaces that exhibited certain nanoscale roughness and/or charge heterogeneity properties. However, release with IS reduction or pH increase is only predicted on surfaces with small nanoscale roughness protrusions. The vast majority of remaining colloidal biochar could be recovered after excavating and gently shaking the sand. This implies that recoverable colloidal biochar was liberated when the torque balance was altered during shaking at microscopic roughness or grain-grain contact locations (e.g, their lever arms were continuously changing). The relatively small amount of irreversibly retained colloidal biochar was attributed to crevice and/or charge heterogeneity sites. Humic acid diminished retention by increasing the electrostatic repulsion (the energy barrier) at certain locations. However, it apparently did not have a large influence on the depth of the primary minimum on rough surfaces that is important for transient release to occur.

Our results imply that addition of biochar at the soil surface will result in leaching losses during irrigation, precipitation, and other agronomic management that reduce the solution IS, especially in the presence of dissolved organic matter. This information is needed to better assess the global carbon cycle and carbon sequestration. Besides, biochar is well known to strongly adsorb many contaminants. Consequently, mobile colloidal biochar during leaching events poses a potential risk to the environment that warrants additional research.

Declaration of competing interest

There are no conflicts to declare.

Acknowledgements

This work was supported by the National Natural Science Foundation of China (41771255), National Key Research and Development Program (2017YFD0801503), the Program of “1000-talents Plan” for young researchers, and the International Training Promotion Project for Graduate Students of China Agricultural University.

Appendix A. Supplementary data

Supplementary data to this article can be found online at https://doi.org/10.1016/j.envpol.2020.114068.

References

Adamczyk, Z., Siwek, B., Zembala, M., Belouschek, P., 1994. Kinetics of localized adsorption of colloid particles. Adv. Colloid Interface Sci. 48 (94), 151–280.
ASTM, 2007. Standard Test Method for Chemical Analysis of Wood Charcoal. ASTM International, West Conshohocken. ASTM D1762- 84.
Bradford, S.A., Kim, H., Shen, C.Y., Sasidharan, S., Shang, J.Y., 2017. Contributions of nanoscale roughness to anomalous colloid retention and stability behavior. Langmuir 33 (38), 10094–10105.
Bradford, S.A., Leij, F.J., 2018. Modeling the transport and retention of polydispersed colloidal suspensions in porous media. Chem. Eng. Sci. 192, 972–980.
Bradford, S.A., Torkzaban, S., 2015. Determining parameters and mechanisms of colloid retention and release in porous media. Langmuir 31 (44), 12096–12105.
Bradford, S.A., Torkzaban, S., Kim, H., Simunek, J., 2012. Modeling colloid and microorganism transport and release with transients in solution ionic strength. Water Resour. Res. 48 (9), 77–86.
Bradford, S.A., Torkzaban, S., Leij, F., Simunek, J., 2015. Equilibrium and kinetic models for colloid release under transient solution chemistry conditions. J. Contam. Hydrol. 181, 141–152.
Bradford, S.A., Torkzaban, S., 2013. Colloid interaction energies for physically and chemically heterogeneous porous media. Langmuir 29 (11), 3668–3676.
Bradford, S.A., Torkzaban, S., Shapiro, A., 2013. A theoretical analysis of colloid attachment and straining in chemically heterogeneous porous media. Langmuir 29 (23), 6944–6952.
Chen, C.Q., Li, J., Devries, S.L., Zhang, P.F., Li, X.Q., 2015. Transport of antibiotic resistance plasmids in porous media. Vadose Zone J. 14 (3) https://doi.org/10.2136/vzj2014.06.0068.
Chen, M., Wang, D.J., Yang, F., Xu, X.Y., Xu, N., Cao, X.D., 2017. Transport and retention of biochar nanoparticles in a paddy soil under environmentally-relevant solution chemistry conditions. Environ. Pollut. 230, 540–549.
Chen, M., Alim, N., Zhang, Y., Xu, N., Cao, X., 2018. Contrasting effects of biochar nanoparticles on the retention and transport of phosphorus in acidic and alkaline soils. Environ. Pollut. 239, 562–570.
Chen, G., Liu, X., Su, C., 2012. Distinct effects of humic acid on transport and retention of TiO_2 rutile nanoparticles in saturated sand columns. Environ. Sci. Technol. 46 (13), 7142.
Cheng, D., Liao, P., Yuan, S.H., 2016. Effects of ionic strength and cationic type on humic acid facilitated transport of tetracycline in porous media. Chem. Eng. J. 284, 389–394.
Dong, X.L., Li, G.T., Lin, Q.M., Zhao, X.R., 2017. Quantity and quality changes of biochar aged for 5 years in soil under field conditions. Catena 159, 136–143.
Feke, D.L., Prabhu, N.D., 1985. Kinetics of coupled primary- and secondary-minimum coagulation in colloidal dispersions. Langmuir 1 (6), 691–696.
Fritz, G., Schädler, V., Willenbacher, N., Wagner, N.J., 2002. Electrosteric stabilization of colloidal dispersions. Langmuir 18 (16), 6381–6390.
Fisher-Power, L.M., Cheng, T., 2018. Nanoscale titanium dioxide (nTiO(2)) transport in natural sediments: importance of soil organic matter and Fe/Al oxyhydroxides. Environ. Sci. Technol. 52 (5), 2668–2676.
Gregory, J., 1981. Approximate expressions for retarded van der waals interaction. J. Colloid Interface Sci. 83 (1), 138–145.
Grolimund, D., Barmettler, K., Borkovec, M., 2001. Release and transport of colloidal particles in natural porous media 2. Experimental results and effects of ligands. Water Resour. Res. 37 (3), 571–582.
Guggenberger, G., Rodionov, A., Shibistova, O., Grabe, M., Kasansky, O.A., Fuchs, H., Mikheyeva, N., Zrazhevskaya, G., Flessa, H., 2008. Storage and mobility of black carbon in permafrost soils of the forest tundra ecotone in Northern Siberia. Global Change Biol. 14 (6), 1367–1381.
Hahn, M.W., O'Meliae, C.R., 2004. Deposition and reentrainment of Brownian particles in porous media under unfavorable chemical conditions: some concepts and applications. Environ. Sci. Technol. 38 (1), 210–220.
Hwang, G., Gomez-Flores, A., Bradford, S.A., Choi, S., Jo, E., Kim, S.B., Tong, M.P., Kim, H., 2018. Analysis of stability behavior of carbon black nanoparticles in ecotoxicological media: hydrophobic and steric effects. Colloids Surf., A: Physicochem. Eng. Asp. 554, 306–316.
Jacob, T., Eddy, P., Johnson, W.P., 2015. Prediction of nanoparticle and colloid attachment on unfavorable mineral surfaces using representative discrete heterogeneity. Langmuir 31 (34), 9366–9378.
Jansen, B., Kalbitz, K., McDowell, W.H., 2014. Dissolved organic matter: linking soils and aquatic systems. Vadose Zone J. 13 (7) https://doi.org/10.2136/vzj2014.05.0051.
Joseph, S.D., Graber, E.R., Chia, C., Munroe, P., Donne, S., Thomas, T., Nielsen, S., Marjo, C., Rutlidge, H., Pan, G.X., Li, L., Taylor, P., Rawal, A., Hook, J., 2013. Shifting paradigms: development of high-efficiency biochar fertilizers based on nanostructures and soluble components. Carbon Manag. 4 (3), 323–343.
Kalra, Y.P., 1997. Handbook of reference methods for plant analysis 38 (6), 1710–1711.
Kretzschmar, R., Sticher, H., 1997. Transport of humic-coated iron oxide colloids in a sandy soil: influence of Ca^{2+} and trace metals. Environ. Sci. Technol. 31 (12),

3497–3504.
Lehmann, J., Joseph, D.S., 2015. Biochar for Environmental Management: Science, Technology and Implementation, 2nd. Routledge Press, London, pp. 15801–15811.
Li, T.T., Jin, Y., Huang, Y.F., Li, B.G., Shen, C.Y., 2017. Observed dependence of colloid detachment on the concentration of initially attached colloids and collector surface heterogeneity in porous media. Environ. Sci. Technol. 51 (5), 2811–2820.
Li, Y.S., Wang, Y.G., Pennell, K.D., Abriola, L.M., 2008. Investigation of the transport and deposition of fullerene (C60) nanoparticles in quartz sands under varying flow conditions. Environ. Sci. Technol. 42 (19), 7174–7180.
Liu, C.-H., Chu, W.Y., Li, H., Boyd, S.A., Teppen, B.J., Mao, J.D., Lehmann, J., Zhang, W., 2019. Quantification and characterization of dissolved organic carbon from biochars. Geoderma 335, 161–169.
Louie, S.M., Phenrat, T., Small, M.J., Tilton, R.D., Lowry, G.V., 2012. Parameter identifiability in application of soft particle electrokinetic theory to determine polymer and polyelectrolyte coating thicknesses on colloids. Langmuir 28 (28), 10334–10347.
Major, J., Lehmann, J., Rondon, M., Goodale, C., 2010. Fate of soil-applied black carbon: downward migration, leaching and soil respiration. Global Change Biol. 16 (4), 1366–1379.
Manyà, J.J., 2012. Pyrolysis for biochar purposes: a review to establish current knowledge gaps and research needs. Environ. Sci. Technol. 46 (15), 7939–7954.
Morales, V.L., Zhang, W., Gao, B., Lion, L.W., Bisogin Jr., J.J., Mcdonough, B.A., Steenhuis, T.S., 2011. Impact of dissolved organic matter on colloid transport in the vadose zone: deterministic approximation of transport deposition coefficients from polymeric coating characteristics. Water Res. 45 (4), 1691–1701.
Murray, J., Keith, A., Singh, B., 2015. The stability of low- and high-ash biochars in acidic soils of contrasting mineralogy. Soil Biol. Biochem. 89, 217–225.
Pazmino, E., Trauscht, J., Johnson, W.P., 2014. Release of colloids from primary minimum contact under unfavorable conditions by perturbations in ionic strength and flow rate. Environ. Sci. Technol. 48 (16), 9227–9235.
Qi, F.J., Kuppusamy, S., Naidu, R., Bolan, N.S., Yong, S.O., Lamb, D., Li, Y.B., Yu, L.B., Semple, K.T., Wang, H.L., 2017. Pyrogenic carbon and its role in contaminant immobilization in soils. Crit. Rev. Environ. Sci. Technol. 47 (10), 795–876.
Rasmuson, A., VanNess, K., Ron, C.A., Johnson, W.P., 2019. Hydrodynamic versus surface interaction impacts of roughness in closing the gap between favorable and unfavorable colloid transport conditions. Environ. Sci. Technol. 53 (5), 2450–2459.
Rechberger, M.V., Kloss, S., Rennhofer, H., Tintner, J., Watzinger, A., Soja, G., Lichtenegger, H., Zehetner, F., 2017. Changes in biochar physical and chemical properties: accelerated biochar aging in an acidic soil. Carbon 115, 209–219.
Redman, J.A., Walker, S.L., Elimelech, M., 2004. Bacterial adhesion and transport in porous media: role of the secondary energy minimum. Environ. Sci. Technol. 38 (6), 1777–1785.
Roy, S.B., Dzombak, D.A., 1997. Chemical factors influencing colloid-facilitated transport of contaminants in porous media. Environ. Sci. Technol. 31 (3), 656–664.
Roy, S.B., Dzombak, D.A., 1996. Colloid release and transport processes in natural and model porous media. Colloids Surf., A: Physicochem. Eng. Asp. 107, 245–262.
Ryan, J.N., Elimelech, M., 1996. Colloid mobilization and transport in groundwater. Colloids Surf., A: Physicochem. Eng. Asp. 107, 1–56.
Ryan, J.N., Gschwend, P.M., 1994. Effects of ionic strength and flow rate on colloid release: relating kinetics to intersurface potential energy. J. Colloid Interface Sci. 164 (1), 21–34.
Sen, T.K., Khilar, K.C., 2006. Review on subsurface colloids and colloid-associated contaminant transport in saturated porous media. Adv. Colloid Interface Sci. 119 (2–3), 71–96.
Sigmund, G., Jiang, C.J., Hofmann, T., Chen, W., 2018. Environmental transformation of natural and engineered carbon nanoparticles and implications for the fate of organic contaminants. Environ. Sci. Nano. 5 (11), 2500–2518.
Shen, C.Y., Bradford, S.A., Li, T.T., Li, B.G., Huang, Y.F., 2018. Can nanoscale surface charge heterogeneity really explain colloid detachment from primary minima upon reduction of solution ionic strength? J. Nano Res. 20 (6), 165. https://doi.org/10.1007/s11051-018-4265-8.
Shen, C.Y., Lazouskaya, V., Zhang, H.Y., Wang, F., Li, B.G., Jin, Y., Huang, Y.F., 2012. Theoretical and experimental investigation of detachment of colloids from rough collector surfaces. Colloids Surf., A: Physicochem. Eng. Asp. 410 (18), 98–110.
Shen, C.Y., Li, B.G., Huang, Y.F., Jin, Y., 2007. Kinetics of coupled primary- and secondary-minimum deposition of colloids under unfavorable chemical conditions. Environ. Sci. Technol. 41 (20), 6976–6982.
Smider, B., Singh, B., 2014. Agronomic performance of a high ash biochar in two contrasting soils. Agric. Ecosyst. Environ. 191, 99–107.
Simůnek, J., Saito, H., Sakai, M., Genuchten, T.M., 2008. The HYDRUS-1D software package for simulating the one-dimensional movement of water, heat, and multiple solutes in variably-saturated media. Dep.of Environmental Sciences Univ.of California Riverside 68.
Torkzaban, S., Bradford, S.A., Vanderzalm, J.L., Patterson, B.M., Harris, B., Prommer, H., 2015. Colloid release and clogging in porous media: effects of solution ionic strength and flow velocity. J. Contam. Hydrol. 181, 161–171.
Torkzaban, S., Bradford, S.A., 2016. Critical role of surface roughness on colloid retention and release in porous media. Water Res. 88, 274–284.
Tosco, T., Tiraferri, A., Sethi, R., 2009. Ionic strength dependent transport of microparticles in saturated porous media: modeling mobilization and immobilization phenomena under transient chemical conditions. Environ. Sci. Technol. 43 (12), 4425–4431.
Tufenkji, N., Elimelech, M., 2004. Deviation from the classical colloid filtration theory in the presence of repulsive DLVO interactions. Langmuir 20 (25), 10818–10828.
Tufenkji, N., Miller, G.F., Ryan, J.N., Harvey, R.W., Elimelech, M., 2004. Transport of cryptosporidium oocysts in porous media: role of straining and physicochemical filtration. Environ. Sci. Technol. 38 (22), 5932–5938.
van Oss, C.J., Chaudhury, M.K., Good, R.J., 1988. Interfacial lifshitz-vanderwaals and polar interactions in macroscopic systems. Chem. Rev. 88 (6), 927–941.
van Oss, C.J., 2003. Long-range and short-range mechanisms of hydrophobic attraction and hydrophilic repulsion in specific and aspecific interactions. J. Mol. Recogn. 16 (4), 177–190.
Wang, D., Ai, J., Shen, F., Yang, G., Zhang, Y., Deng, S., Zhang, J., Zeng, Y.M., Song, C., 2017. Improving anaerobic digestion of easy-acidification substrates by promoting buffering capacity using biochar derived from vermicompost. Bioresour. Technol. 227, 286–296.
Wang, D.J., Zhang, W., Hao, X.Z., Zhou, D.M., 2013a. Transport of biochar particles in saturated granular media: effects of pyrolysis temperature and particle size. Environ. Sci. Technol. 47 (2), 821–828.
Wang, D.J., Zhang, W., Zhou, D.M., 2013b. Antagonistic effects of humic acid and iron oxyhydroxide grain-coating on biochar nanoparticle transport in saturated sand. Environ. Sci. Technol. 47 (10), 5154–5161.
Wang, P., Qi, N., Ao, Y., Hou, J., Wang, C., Qian, J., 2016. Effect of UV irradiation on the aggregation of TiO2 in an aquatic environment: influence of humic acid and pH. Environ. Pollut. 212, 178–187.
Wang, Y., Zhang, W., Shang, J.Y., Shen, C.Y., Joseph, S.D., 2019. Chemical aging changed aggregation kinetics and transport of biochar colloids. Environ. Sci. Technol. 53 (14), 8136–8146.
Wang, Y.G., Li, Y.S., Fortner, J.D., Hughes, J.B., Abriola, L.M., Pennell, K.D., 2008. Transport and retention of nanoscale C60 aggregates in water-saturated porous media. Environ. Sci. Technol. 42 (10), 3588–3594.
Wen, Y.C., Guo, X.H., Kalasin, S., Santore, M.M., 2014. Capture of soft particles on electrostatically heterogeneous collectors: brushy particles. Langmuir 30 (8), 2019–2027.
Yan, C.R., Cheng, T., Shang, J., 2019. Effect of bovine serum albumin on stability and transport of kaolinite colloid. Water Res. 155, 204–213.
Yang, G., Wang, Z.H., Xian, Q.M., Shen, F., Sun, C., Zhang, Y.Z., Wu, J., 2015. Effects of pyrolysis temperature on the physicochemical properties of biochar derived from vermicompost and its potential use as an environmental amendment. RSC Adv. 5 (50), 40117–40125.
Yang, W., Bradford, S.A., Wang, Y., Sharma, P., Shang, J.Y., Li, B.G., 2019a. Transport of biochar colloids in saturated porous media in the presence of humic substances or proteins. Environ. Pollut. 246, 855–863.
Yang, W., Shang, J.Y., Sharma, P., Li, B.G., Liu, K.S., Flury, M., 2019b. Colloidal stability and aggregation kinetics of biochar colloids: effects of pyrolysis temperature, cation type, and humic acid concentrations. Sci. Total Environ. 658, 1306–1315.
Yang, W., Wang, Y., Sharma, P., Li, B.G., Liu, K.S., Liu, J., Flury, M., Shang, J.Y., 2017a. Effect of naphthalene on transport and retention of biochar colloids through saturated porous media. Colloids Surf., A: Physicochem. Eng. Asp. 530, 146–154.
Yang, W., Wang, Y., Shang, J.Y., Liu, K.S., Sharma, P., Liu, J., Li, B.G., 2017b. Antagonistic effect of humic acid and naphthalene on biochar colloid transport in saturated porous media. Chemosphere 189, 556–564.
Zhang, W., Niu, J.Z., Morales, V.L., Chen, X.C., Hay, A.G., Lehmann, J., Steenhuis, T.S., 2010. Transport and retention of biochar particles in porous media: effect of pH, ionic strength, and particle size. Ecohydrology 3 (4), 497–508.
Zhou, D.D., Ghosh, S., Zhang, D., Liang, N., Dong, X.D., Wu, M., Pan, B., 2016. Role of ash content in biochar for copper immobilization. Environ. Eng. Sci. 33 (12) https://doi.org/10.1089/ees.2016.0042.